

Supporting materials for

Ferromagnetic Topological Insulator in Two-Dimensional

Honeycomb Lattice

Hao Wang¹, Ning Mao¹, Chengwang Niu¹, Shiyong Shen¹, Myung-Hwan Whangbo^{2,3,4}, Baibiao Huang² and Ying Dai¹

¹School of Physics, Shandong University, Jinan 250100, China

²School of Physics, State Key Laboratory of Crystal Materials, Shandong University, Jinan 250100, China

³Department of Chemistry, North Carolina State University, Raleigh, North Carolina 27695-8204, USA

⁴State Key Laboratory of Structural Chemistry, Fujian Institute of Research on the Structure of Matter, Chinese Academy of Sciences, Fuzhou, Fujian, 350002, P. R. China

Corresponding authors: c.niu@sdu.edu.cn (C. Niu), daiy60@sdu.edu.cn (Y. Dai)

The zigzag edge states

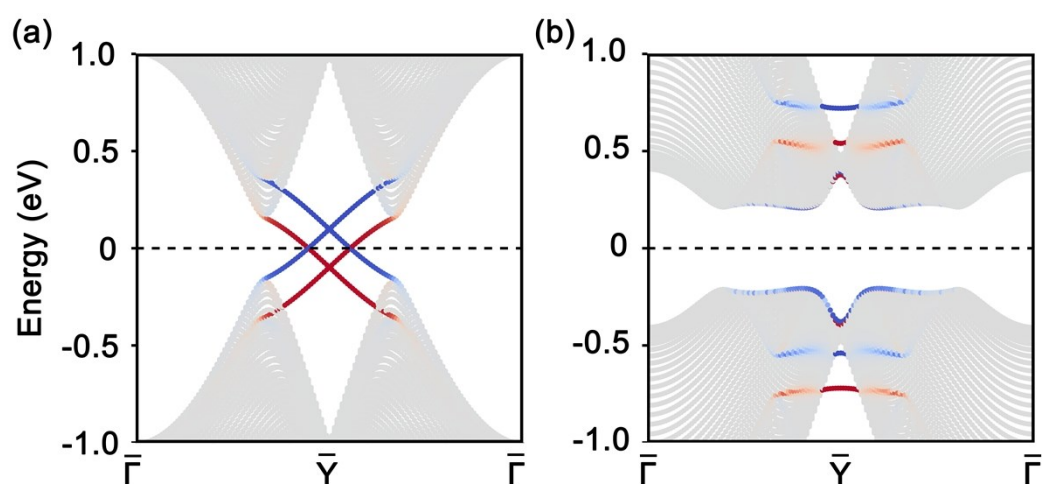


Figure S1. The zigzag edge states for the time-reversal-invariant TIs (a) and time reversal-broken TIs (b), respectively.

The molecular dynamics simulations

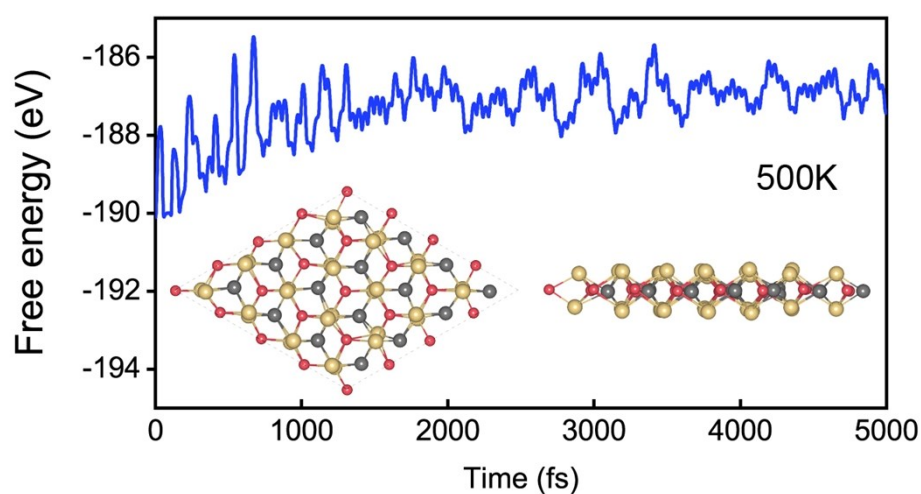


Figure S2 Thermal stability. The molecular dynamics simulations of two-dimensional (2D) Na_2MnPb under 500K. The total time is 5 ps, and the time step is 1 fs. The insets show the snapshots of the structure at 5ps.

The Berry curvature

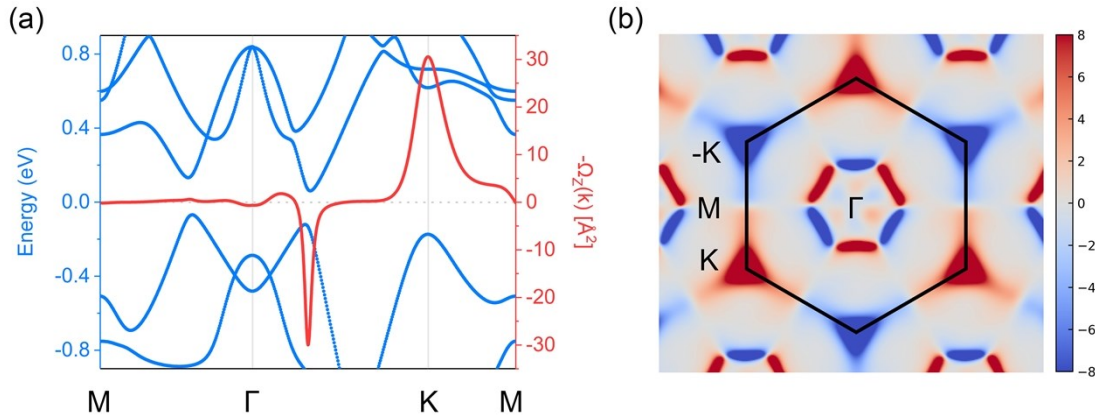


Figure S3 Berry curvature. (a) Red line denotes the Berry curvature along M- Γ -K-M path with the in-plane magnetization. (b) 2D Berry curvature of SL Na₂MnPb with in-plane magnetization, the black line respect for the first Brillouin zone. The colors stand for the values of the Berry curvatures. The even function characters of the Berry curves result in the Chern number is zero, indicating that Na₂MnPb would not be a quantum anomalous Hall insulator.

The effect of Hubbard U

Owing to the strong correlated d electrons of Mn atoms, the GGA+U method is used to correct the strong Coulomb repulsive interactions with effective U parameters from 1eV to 5eV are included in our self-consistent calculations, which are in a reasonable range of Mn atom¹. Figures S4 (a) and (b) present the band structures with different U values for in-plane and out-of-plane magnetization, respectively. Clearly, although the bandgaps and band dispersions can be slightly tuned, the topological nontrivial characters remain intact for all considered U values.

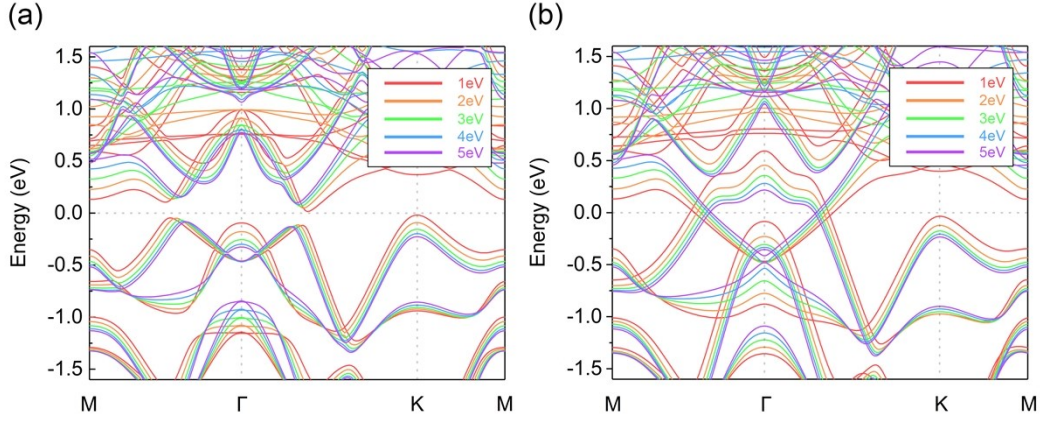


Figure S4 Effects of Hubbard U parameters. The band structures of SL Na_2MnPb vary with the effective Hubbard U parameters under (a) in-plane ferromagnetism and (b) out-of-plane ferromagnetism.

The calculation of J_1

The spin Hamiltonian can be written as: $H = -\sum_{\langle i,j \rangle} J_1 \vec{S}_i \cdot \vec{S}_j - \sum_{\langle\langle i,j \rangle\rangle} J_2 \vec{S}_i \cdot \vec{S}_j$, where $\langle i, j \rangle$ and $\langle\langle i, j \rangle\rangle$ stand for the nearest and next-nearest sites, J_1 and J_2 are the nearest-neighbor and next-nearest-neighbor, respectively. Thus, the total energy of different magnetic configurations (scheme in Figure S5) are:

$$E_{FM} = E_0 - (12J_1 + 12J_2) \times \left| \vec{S}^r \right|^2$$

$$E_{sAFM} = E_0 - (-4J_1 - 4J_2) \times \left| \vec{S}^r \right|^2$$

$$E_{zAFM} = E_0 - (-4J_1 + 4J_2) \times \left| \vec{S}^r \right|^2$$

Here, $\left| \vec{S}^r \right| = \frac{5}{2}$, and the E_{FM} , E_{sAFM} , E_{zAFM} are the total energy of FM, stripy AFM and zigzag-AFM configurations, respectively. Combining these equations, we can deduce

$$J_1 = \frac{1}{16 \left| \vec{S}^r \right|^2} (2E_{zAFM} - E_{FM} - E_{sAFM}), \quad \sqrt{3} \times 2 \text{ supercell is adopt to calculate all of these}$$

magnetic configuration, and the calculated J_1 is 1.558 meV.

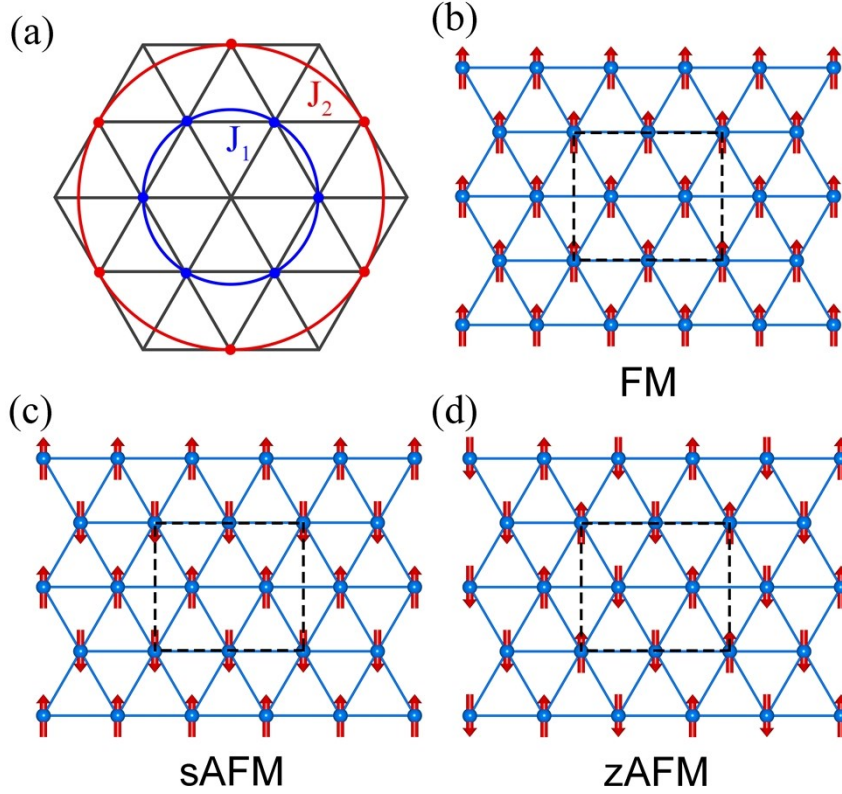


Figure S5 (a) J_1 and J_2 are the nearest-neighbor and next nearest-neighbor exchange energies. The scheme of different magnetic configurations: (b) FM, (c) stripe AFM, and (d) zigzag-AFM, respectively. The dashed line stand for the $\sqrt{3} \times 2$ supercell.

The Monte Carlo simulation of 2D XY model

According to $T_c = \frac{0.89}{k_B} J_1$ of BKT transition, the predicted critical temperature is

about 16K, which is in good agreement with our MC simulations for 2D XY model. As shown in Figure S6, the peak position of the heat capacity is 18 K at the lattice size of 100×100 . This transition temperature indicates that the long-range ordered phase is possible to be observed in current experimental conditions.

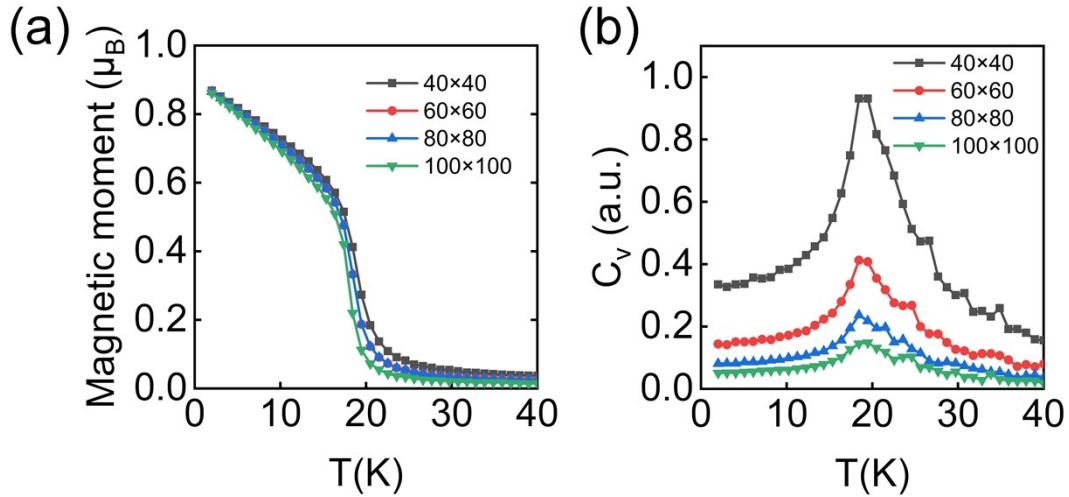


Figure S6 The calculated magnetic moment (a) and heat capacity (b) as a function of temperature for the 2D XY model. The different color of dots stands for the different lattice size of MC lattice (size=40, 60, 80, 100). The peak position of the heat capacity can be regard as the critical temperature of BKT transition. The MC simulation are implemented with 80000 step to reach the thermal equilibrium; the physical quantities are obtained with the average values of 160000 steps to reduce fluctuations. (Noted that the S quantum number of BKT model is 1, which is different from the magnetic moment of SL Na_2MnPb)

The spectrum of P_x operator

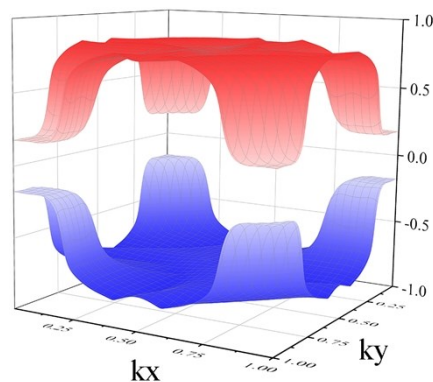


Figure S7. The spectrum of P_x for the spin-up (+1) and spin-down (-1) manifold in the first Brillouin zone. Due to the SOC, the eigenvalues of the P_x are not strictly 1 or -1 owing to the spin is not a good quantum number, but it is clear that there is a gap

between the spin-up and spin-down manifold.

The $k \cdot p$ model

To better understand the topological nature near the Γ point, we write a model Hamiltonian to capture the nature of the low-energy excitation using the $k \cdot p$ method². As mentioned above, the crossing bands are mainly contributed by the Mn- d_{z^2} and Pb- $p_{x,y}$ orbitals. So we consider the $\left| \frac{3}{2}, \frac{3}{2} \right\rangle$, $|d_{z^2}, \uparrow\rangle$, $\left| \frac{3}{2}, -\frac{3}{2} \right\rangle$, and $|d_{z^2}, \downarrow\rangle$ as the basis vector, where $\left| \frac{3}{2}, \frac{3}{2} \right\rangle$ represents the $\frac{1}{\sqrt{2}}(|p_x, \uparrow\rangle + i|p_y, \uparrow\rangle)$ and $\left| \frac{3}{2}, -\frac{3}{2} \right\rangle$ represents the $\frac{1}{\sqrt{2}}(|p_x, \downarrow\rangle + i|p_y, \downarrow\rangle)$. The Hamiltonian can be written in the form of Dirac Γ_i matrices as $\hat{H}_0 = \varepsilon(k)I + \sum_i d_i(k)\Gamma_i$, where I is the identity matrices and Γ_i are the Dirac matrices. In two dimensions, we set k_z as zero. By expanding the k polynomial only up to quadratic order, we can write our model Hamiltonian as

$$\hat{H}_{eff} = \begin{Bmatrix} M_0 + M_1 k^2 & Ak_+ & 0 & Ck_- \\ Ak_- & -M_0 - M_1 k^2 & Ck_- & 0 \\ 0 & Ck_+ & M_0 + M_1 k^2 & Ak_- \\ Ck_+ & 0 & Ak_+ & -M_0 - M_1 k^2 \end{Bmatrix},$$

where $k_{\pm} = k_x \pm ik_y$, $k^2 = k_x^2 + k_y^2$. By fitting the band structures of the model Hamiltonian with that of the first-principles calculations, we obtain the parameters M_0 and M_1 to be -0.43 and 0.24, respectively. The constants A and C determine the effect of the exchange interactions and are used to tune the spin orientations by changing the

relative values of A and C . In the main manuscript, **Fig. 5e** presents the polar angle dependent band structure derived from our model Hamiltonian. When $C = 0$, the in-plane ferromagnetism opens a band gap with the maximum values. With increasing the value of C , the spin orientation changes from the in-plane to the out-of-plane, and the bandgap decreases and closes only when the magnetization is oriented along the out-of-plane direction, illustrated in **Fig. 5e** and **5f**. Therefore, the results of first-principles calculations are well reproduced by the model Hamiltonian.

Table S1. Magnetic anisotropy energy (MAE) of single layer Na_2MnPb from VASP and Fleur codes with different density of k-mesh. The in-plane direction is shown to be energetically preferred.

	12×12×1	15×15×1	18×18×1	21×21×1	24×24×1
MAE(meV/Mn)					
VASP code	8.07	9.28	9.46	9.27	9.22
MAE(meV/Mn)					
Fleur code	10.13	10.51	9.74	9.59	9.55

Table S2. The energy difference, band gap and spin Chern number with different directions of in-plane magnetization for single layer Na_2MnPb .

	0°	30°	60°	90°

ΔE (μeV)	0	2.4	4.4	2.3
band gap (meV)	129.1	130.0	129.1	127.5
spin Chern number	1	1	1	1

References

- [1] J. H. Lee, K. M. Rabe, Phys. Rev. Lett., 2010, **104**, 207204.
- [2] C. X. Liu, X. L. Qi, H. J. Zhang, X. Dai, Z. Fang, S. C. Zhang, Phys. Rev. B, 2010, **82**, 045122.
- [3] S. Q. Zhang, R. Z. Xu, W. H. Duan, X. L. Zou, Adv. Func. Mater., 2019, **29**, 1808380.
- [4] H. L. Zhuang, R. G. Hennig, Phys. Rev. B, 2016, **93**, 054429
- [5] M. Ashton, D. Gluhovic, S. B. Sinnott, J. Guo, D. A. Stewart, R. G. Hennig, Nano Lett., 2017, **17**, 5251
- [6] N. D. Mermin, H. Wagner, Phys. Rev. Lett., 1966, **17**, 1133
- [7] J. M. Kosterlitz, D. J. Thouless, 1973, J. Phys. C: Solid State Phys., **6**, 1181